INTERNATIONAL JOURNAL OF HYDROGEN ENERGY 44 (2019) 26469–26476

Available online at www.sciencedirect.com

ScienceDirect

journal homepage: www.elsevier.com/locate/he

First-principles study of bubble formation and cohesion properties of hydrogen at Fe/W interfaces

Qian Wang [a,b], Guoping Du [a,*], Nan Chen [a,**], Changshuang Jiang [a]

[a] School of Materials Science and Engineering, Nanchang University, Nanchang, Jiangxi, 330031, China
[b] School of Environmental and Chemical Engineering, Nanchang Hangkong University, Nanchang, Jiangxi, 330063, China

HIGHLIGHTS

- Hydrogen at Fe/W interface has a negative binding energy.
- The hydrogen solubility of Fe/W interface is bigger than W and Fe bulks with the increasing temperature.
- The location of hydrogen has an important role on cohesion properties of Fe/W interface.
- Our simulations agree well with similar experimental observations in the literature.

ARTICLE INFO

Article history:
Received 15 April 2019
Received in revised form
6 August 2019
Accepted 11 August 2019
Available online 6 September 2019

Keywords:
Thermodynamic stability
Hydrogen solubility
Interface cohesion
Fe/W interfaces
First-principles study

ABSTRACT

First-principles study is used to comparatively investigate the mechanism of bubble formation of hydrogen at Fe/W interfaces and the effects of H on interface cohesion. It is found that hydrogen at interfacial sites has a negative binding energy, which is quite different from W and Fe bulks with interstitial hydrogen. The hydrogen solubility of the interface is bigger than W and Fe bulks with the increasing temperature, predicting that the Fe/W interface can more easily trap hydrogen and rapidly form bubbles. In addition, we also reveal the sites of hydrogen have an important role on cohesion properties of Fe/W interface, and that the obvious increase of interface strength and stability have been found in the locations of hydrogen relatively far away the center between Fe and W interface layers. The derived results are discussed extensively through comparing with available observations in the literature, and could give a deep understanding of hydrogen at Fe/W interfaces.

Introduction

During the past decades, tungsten (W) is gaining increasing attention for potential applications in fusion reactors [1–4]. It has been selected as one of promising candidates for plasma-facing component (PFC) due to its high melting point, outstanding mechanical properties, low sputtering yield and erosion rate, high resistance to wear and so on [5–8]. It is well known that iron (Fe) is an important structure material connecting to W components under a fusion environment [9,10], and the performance of W–Fe interfaces has fundamental effects on the lifetime of PFC. In this respect, the interface

* Corresponding author.
** Corresponding author.
E-mail addresses: guopingdu@ncu.edu.cn (G. Du), nanchen@ncu.edu.cn (N. Chen).
https://doi.org/10.1016/j.ijhydene.2019.08.070
0360-3199/

strength, work function and magnetic properties of various W–Fe interfaces have been recently derived by means of experimental and calculated methods [11–13].

Hydrogen (H) and its isotopes should be abundant in PFC during the process of fusion reactions, and would accumulate and form bubbles in W bulks and Fe/W interfaces [14–16]. H blistering formation in PFC is an important concern, some experimental and theoretical researchers performed many methods to explain the mechanism controlling bubble formation. These studies have been mainly focused on the solubility and diffusivity of H at W and its alloy bulks [17,18], which find out that H should accumulate easily by defects such as vacancies and grain boundaries [19,20]. As to the solubility of H at Fe/W interfaces, however, there is no any research report in the literature to the best of our knowledge. In addition, H at interfacial site has significant implications of work function and interface strength, and it is essential to investigate the effects of locations of hydrogen on the performance parameters of Fe/W interfaces.

By means of highly accurate first principles study based on density functional theory, we perform a detailed study on bubble formation and cohesion properties of H at Fe/W interfaces. In this study, first-principles study will be combined with the Sievert's law, to predict the temperature-dependent solubility of hydrogen at Fe/W interfaces. The H solubility of W and Fe bulks are also derived for the sake of comparison. Moreover, we also investigate the effects of interstitial H on interface strength and work function. It will be shown that the derived results are not only in good agreement with experimental results in the literature, but also provide a deep understanding of H behaviors of Fe/W interfaces, as well as W and Fe bulks.

Computational methods

The first-principles study is based on the plane-wave pseudopotential total energy method as implemented in the Vienna ab initio simulation package (VASP) [21,22]. We use generalized gradient approximation (GGA) to describe electronic exchange and correlation terms [23,24]. Electron-ion interaction is handled by projector augmented wave (PAW) method [25]. In each calculation, periodic boundary conditions are fixed in all three principal axes, and the supercell is fully relaxed with respect to structural volume and atomic coordinates. In the present work, the cutoff energy is up to 400 eV for a plane-wave basis. For k space integration, the Methfessel-Paxton smearing method [26] is chosen for relaxation calculations, and the tetrahedron method [27] with Blöchl corrections is adopted for static calculations. The Gamma-centered k grids of $9 \times 9 \times 1$ and $11 \times 11 \times 1$ mesh is sampled for the relaxation and static calculations, respectively. The force criterion acting on each atom during relaxation is 1.0×10^{-3} eV/Å, and the criteria of energy convergence are 2.0×10^{-6} eV/atom.

The sandwich model of Fe/W is constructed between low-index surface of (100) of body-centered cubic (bcc) Fe (overlayer) and W (substrate), and such a selection is mainly due to excellent interfacial binding properties [12]. A surface 2×2 (4 atoms) unit cell with the optimized lattice constant of W bulk ($a = 3.172$ Å) is selected for the present structure, which has 7 W and $(5 + 5)$ Fe layers with a vacuum distance of $(15 + 15)$ Å, respectively. In particular, the magnetic spin-polarized method is adopted for Fe overlayers. To predict bubble formation and cohesion properties of H at (100)Fe/(100)W interface, one H atom is added at the octahedral (O) and tetrahedral (T) interstitial sites of each interface, and Fig. 1 shows all interstitial sites of H at Fe/W interface.

We take into account the Zero-point energy (*ZPE*) of H at Fe/W interface, and the *ZPE* of H atom can be calculated as:

$$E_{ZPE} \approx \frac{1}{2}\sum_{I} \hbar\nu_i \tag{1}$$

where $\hbar$ and ν_i are Plank's constant and the normal vibration frequencies. The mass of H atom has much lighter than that of metal atoms of W and Fe, which results in that huge differences of frequencies of between H and W or Fe. Accordingly, *ZPE* is derived only from normal vibrational modes of H, and the metal atoms are kept immobile.

In addition, the binding energy (E_b) is adopted to predict thermodynamic stability of H atom. The work of separation (W_{sep}) and interface energy (E_{int}) are as parameters to express the interfacial strength and interface stability, respectively. Specifically, the lower binding energy, work of separation and interface energy signify the more stable interfacial H atom, weaker interfacial strength and more stable interface, respectively. The detailed investigations of H at Fe/W interfaces will be discussed in the following paragraphs.

Results and discussion

Thermodynamic stability

Prior to the calculation, the all possible locations of H at (100) Fe/(100)W interface are considered. As illustrated in Fig. 1, eleven interstitial sites with H have been examined in our calculations, i.e., six octahedral (O1–O6) and five tetrahedral sites (T1-T5). It can be observed clearly from this figure that the sites of O1–O3 and T1-T2 are located at W lattices, the sites of O4–O6 and T4-T5 are at Fe lattices, and T3 site is at M plane between W and Fe layers. Specifically, there are two kinds of O sites for W and Fe layers, i.e., O2, O3, O4 and O5 with different encircling atoms of W and Fe, as shown obviously in Fig. 1(b) and (c). After full relaxation, it is found that H could not stay at some interstitial sites, that is to say, H is energetically unstable at O3 site and has relaxed to the neighboring T1 site, and that the sites of O5、T3 and T4 relaxed to T5 site.

The solubility is related to thermodynamic stability of H at Fe/W interface, accordingly, the binding energy (E_b) of H at all interstitial sites must be discussed. The E_b without the ZPE corrections is defined as the following formula:

$$E_b = \frac{1}{2}\left(E_{Fe/W-H} - E_{Fe/W} - E_{H_2}\right) \tag{2}$$

and the corresponding E_b with consideration of *ZPE* theory is expressed by:

$$E_b = \frac{1}{2}\left(E_{Fe/W-H} + E^{ZP}_{Fe/W-H} - E_{Fe/W} - E_{H_2} - E^{ZP}_{H_2}\right) \tag{3}$$

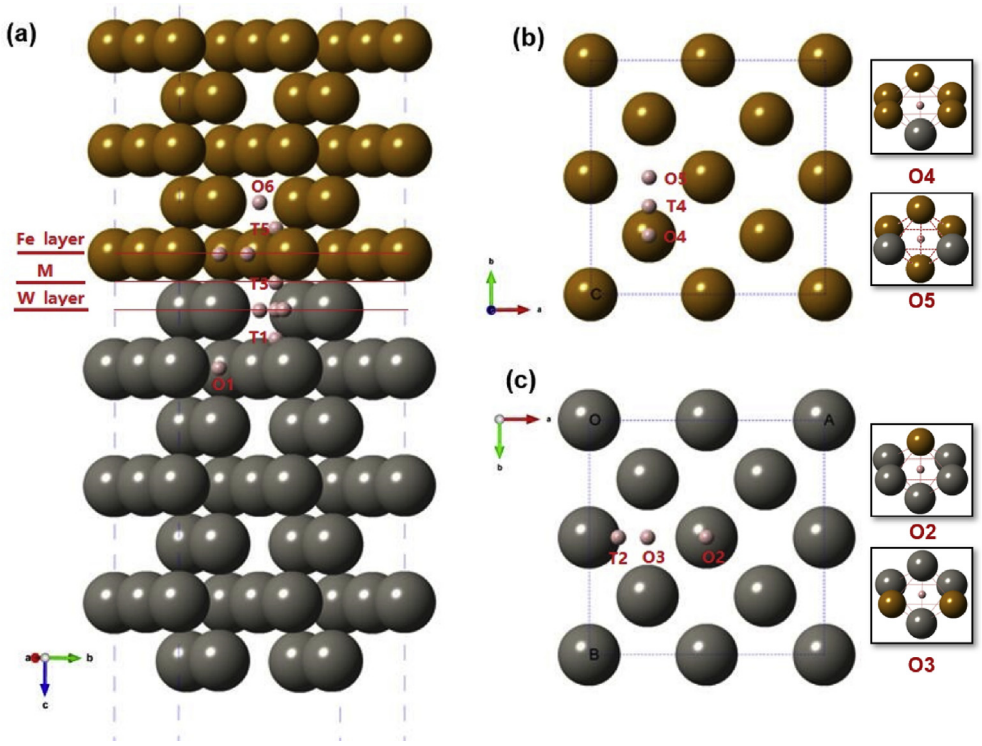

Fig. 1 – Schematic illustrations of octahedral (O1–O6) and tetrahedral (T1-T5) interstitial sites of hydrogen at (100)Fe/(100)W interface. (a) three-dimensional structure of Fe/W interface, (b) a bottom view of x-y projection of Fe layer, and (c) a top view of x-y projection of W layer. The big gray, middle yellow, and small pink balls represent W, Fe, and H atoms, respectively. The M plane is just at the center of the interface layers between Fe and W. (For interpretation of the references to color in this figure legend, the reader is referred to the Web version of this article.)

Here, $E_{Fe/W-H}$ and $E_{Fe/W}$ stand for total energies of the sandwich model of Fe/W with and without H atoms, respectively. E_{H_2} represents total energy of H_2 molecule, $E^{ZP}_{Fe/W-H}$ is ZPE of H at the interfaces, and $E^{ZP}_{H_2}$ is ZPE of H_2 molecule.

We first obtain the *ZPE* and E_b of H at O and T sites of bcc W and Fe bulks as a reference, which are listed in Table 1. In particular, the supercells of $3 \times 3 \times 3$ (54 atoms) are selected for the bulk calculations of W and Fe, respectively. Then, in the present of interfacial calculations, the *ZPE* and E_b of H at all interstitial sites are derived (see Table 1). The E_b values of bulks in Table 1 show that the present results are in fair agreement with the computed and experimental data in the literature [28–33]. For instance, the E_b value of H at T site of W bulk with *ZPE* is found to be 0.901 eV, which is consistent with the corresponding data (1.04 and 0.89 eV) from theory [32] and experiment [33], respectively. In addition, the present *ZPE* (0.129 eV, T site and 0.237 eV, O site) of H at Fe bulk are also consistent with the calculated values of 0.134 and 0.251 eV, respectively [28]. All above agreements indicate that H behaviors of Fe/W interface can be accurately revealed by PAW-GGA method.

Consequently, several features on the thermodynamic stability of H at Fe/W interface can be observed from Table 1. Firstly, it can be discerned clearly from Table 1 that the E_b value of T5 site in Fe lattice (−0.137 eV) is lower than that of the sites of O4 and O6 (0.971 and 0.473 eV), and the same situation can be applicable for W lattice of this interface. Such a direct comparison implies that the T site should be

Table 1 – Zero-point energy (*ZPE*) and binding energies (E_b) of interstitial hydrogen at (100)Fe/(100)W interfaces, as well as W and Fe bulks. The corresponding experimental and calculated data in the literature are also listed for comparison.

Type	H location	*ZPE* (eV/atom)	E_b (eV)	
			without *ZPE*	with *ZPE*
Fe/W interface	T1	0.251	0.619	0.61
	T2	0.248	0.526	0.514
	T5	0.155	−0.137	−0.242
	O1	0.134	0.979	0.853
	O2	0.133	0.828	0.701
	O4	0.158	0.971	0.869
	O6	0.149	0.473	0.362
Fe bulk	T	0.237	0.135	0.112
		Cal. 0.251[a]	Cal. 0.2[a]	Exp. 0.29[b]
	O	0.129	0.264	0.133
		Cal. 0.134[a]	Cal. 0.33[a]	–
W bulk	T	0.265	0.896	0.901
		Cal. 0.26[c]	Cal. 0.90[d], 0.89[e]	Exp. 1.04[f]
	O	0.151	1.279	1.17
		Cal. 0.15[c]	Cal. 1.29[e], 1.30[d]	–

[a] Ref. [28].
[b] Ref. [29].
[c] Ref. [30].
[d] Ref. [31].
[e] Ref. [32].
[f] Ref. [33].

thermodynamically more stable than the O site for H at Fe/W interface, which is the same from the stable T site of W and Fe bulks. The phenomenon suggests that the formation of Fe/W interface has a negligible effect on the favorable location of H. Secondly, the T5 site has the lowest E_b value of −0.137 eV among the bulks and interfaces, signifying that H at T5 site is energetically more favorable than the others, i.e., the generated H would rapidly accumulate at T5 site along fusion reactions. In addition, the O1 site with *ZPE* would to be more stable with lower E_b value than O4 site, which is entirely opposed to the conclusion without *ZPE* corrections. Such a phenomenon suggests that *ZPE* theory seems important to be included for the study of thermodynamic stability of H at Fe/W interface.

Since work function (Φ) is proportional to electron density, and it is of importance to have a deep understanding of hydrogen at interstitial sites from work function scale. Accordingly, the work functions of hydrogen at Fe/W interface are next derived by the following equation:

$$\Phi = V_{vac} - E_f \tag{4}$$

where V_{vac} and E_f represent the vacuum potential and Fermi energy of this interface, respectively. Fig. 2 demonstrates work functions of H at the sites of T1 and O1 in W lattice as a typical example. We also calculated and show the work function of pure Fe/W interface (3.99 eV) in the figure for comparison. The value from pure interface matches well similar computed value in the literature [12], which presents the creditability of the other Φ values. It is interesting to observe that the Φ values of H at Fe/W interface are smaller than pure interface, predicting that the releasing electron is promoted by the generated H in fusion reactions. More importantly, the Φ value of T1 site is higher than the corresponding O1 site for W lattice. Such a coincidence suggests that a strong correlation between work function and interstitial sites of H at Fe/W interface could be found, i.e., the more stable site should have higher work function, and vice versa.

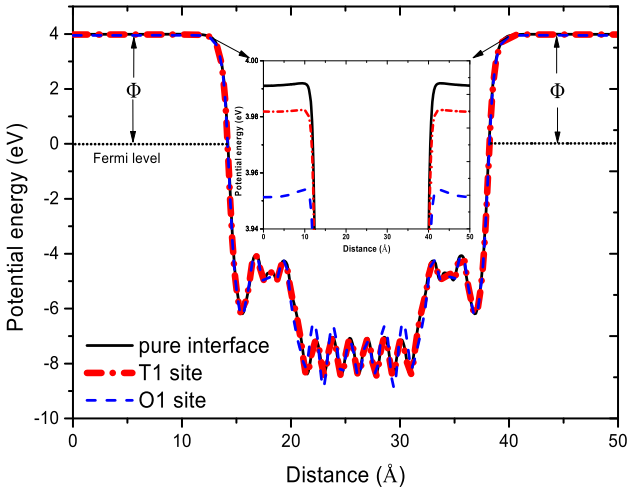

Fig. 2 – Work function (Φ) of (100)Fe/(100)W interface with hydrogen at T1 and O1 sites of W lattice, and the Φ of pure Fe/W interface is also shown in the figures for comparison.

Hydrogen solubility

In order to further understand the H accumulation and bubble formation of Fe/W interface, according to thermodynamics and Sievert's law, temperature-dependent solubility (C-T) of H at Fe/W interface can be defined as follows:

$$C = K_S\sqrt{P} \tag{5}$$

Here, P represents the H pressure in the gas phases, and P = 1 atm in this work. K_S is the Sieverts' constant and has been given as [34,35]:

$$K_S = \exp\left(\beta\left[\sum_i \frac{h\gamma_i}{4} - E_b - \frac{1}{2}\sum_i h\nu_i\right]\right) \frac{1}{\sqrt{\alpha}}\sqrt{1-\exp\left(-\beta\sum_i \frac{h\gamma_i}{2}\right)}\ \frac{1}{\prod_i(1-e^{-\beta h\nu_i})} \tag{6}$$

where $\alpha = \left(\frac{2\pi m k_B T}{h^2}\right)^{3/2}\frac{4\pi^2 I(k_B T)^2}{h^2}$ and $\beta = \frac{1}{k_B T}$, E_b and ν_i have the same meanings as shown in Eqs. (1) and (2), respectively, γ_i is vibration frequency of gaseous H_2, m and I denote the mass and moment of inertia of H_2, respectively. It should be pointed out that the Sieverts' constant of the interface is obtained by means of the summation of K_S values of all the interstitial sites.

After a series of calculations, Fig. 3 shows the temperature-dependent solubility of H at (100)Fe/(100)W interface, as well as W and Fe bulks. Generally speaking, excellent agreement with experimental observation is a kind of criterion to confirm theoretical calculation. Thus, the H solubility of bulk W from similar experimental and calculated methods are also listed in this figure for the sake of comparison. One can observe from Fig. 3 that our predicted H solubility of bulk W agrees well with the corresponding experimental and calculated values with the increasing temperature [32,33]. Specific to see, all the predictions from theoretical calculations seem to be a bit

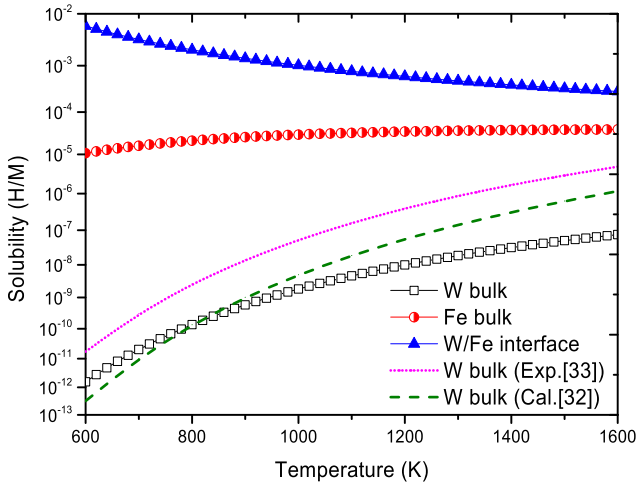

Fig. 3 – Temperature-dependent solubility of hydrogen at (100)Fe/(100)W interfaces, as well as Fe and W bulks. The experimental and calculated values of W bulk in the literature [32,33] are also included for the sake of comparison.

lower than experimental data [32,33]. In our opinion, the ignored differences might be due to the effects of defects (e.g. vacancies, dislocations and grain boundaries) in the experiments. The present values of W bulk are more close to the experimental data below the temperature of ~900 K [33], and match well with the corresponding data from DFT theory at high temperatures [32]. The above excellent consistency between experimental observation and theoretical calculation confirms that the intrinsic mechanisms of bubble formation of Fe/W interface can be accurately predicted by our works.

According to the current studies, we would give a probably useful insight into the bubble formation of H at Fe/W interface, as well as Fe and W bulks. The solubility of H at W bulk is only 10^{-12}–10^{-9}, much lower than the corresponding Fe bulk in the temperature range 600–1600 K. It follow therefore that H should be difficult to accumulate and form bubbles at W bulk. However, the H concentration of Fe/W interface is slightly higher than the corresponding values of W and Fe bulks in the same temperature range, indicating that Fe–W interaction can promote H dissolution in the bulks. The solubility of H at Fe/W interface even reaches 5.9×10^{-3} at 600K. Such an extremely big value implies the Fe/W interface can more easily trap H and rapidly form H bubbles at this temperature range. In addition, a careful observation from Fig. 3 that the solubility of the interface falls with the increasing temperature, while a growing trend for bulks. In other words, the interface formation of Fe/W has the much smaller effects on the H accumulation and bubble formation at high temperatures.

To understand the effects of the Fe/W interface formation on H dissolution of bulk, the electronic structures of H at interface and bulk are thus analyzed. The comparison of total density of states (TDOS) of H at interfacial T5 site (Fe side) and T site of Fe bulk is plotted in Fig. 4. It can be deduced from this figure that the main TDOS peak of H at T5 site located at about −9.5 eV below the Fermi level (E_f) is much higher than that of H at T site, and that the TDOS values of T5 site have moved leftward to the positions. In addition, to further compare Fe–H interfacial bonds with those formed in bulk, the Bader analysis [36,37] is performed to calculate the bond charges between H and Fe atoms in interfacial T5 and bulk T sites. The bond charge of H atom is 0.376 e in T5 site, which is 0.003 e larger than that of bulk T site. From the above facets it suggests that H at T5 interfacial site should have a stronger chemical bonding than the corresponding T site of Fe bulk.

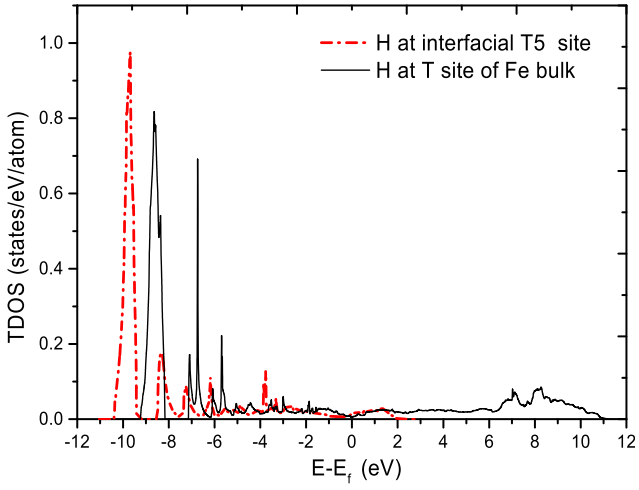

Fig. 4 – Total density of states (TDOS) of hydrogen at interfacial T5 site (Fe side) and T site of Fe bulk.

Interface cohesion

The work of separation (W_{sep}), which is defined as the energy required to reversibly separate the interface into two free surfaces, is readily calculated by [12]:

$$W_{sep} = \frac{E_{Fe-layer} + E_{W-layer} - E_{tot}}{2A} \quad (7)$$

where E_{tot} and A are total energy and surface area of H at Fe/W interface, respectively. $E_{Fe-layer}$ and $E_{W-layer}$ are total energies of overlayer and substrate layers after the removal of the W and Fe, respectively.

According to our calculations, Table 2 summarizes the work of separation (W_{sep}) of (100)Fe/(100)W interface with H at all the seven interstitial sites. The changes of work of separation (ΔW_{sep}) as a reference of pure interface ($W_{sep} = 6.283$ J/m^2) are also calculated and reported in the table for comparison. The present W_{sep} of pure (100)Fe/(100)W interface is in excellent agreement with the computed data given Yang et al. [38] and Ren et al. [12]. As can be seen in Table 2, the W_{sep} and ΔW_{sep} values of H at T5、O1 and O6 sites are higher than the other four sites. Especially, the ΔW_{sep} values of the sites of O1 and O6 are about 0.2 J/m^2 higher than that of the pure interface, suggesting that the interface strength is increased by the two locations of H, which are relatively far away from M plane as shown in Fig. 1. However, H at the left sites of T1、T2、O2 and O4 can reduce the W_{sep} values. One conclusion from this section is that the interstitial sites of H at interface have crucial influence on cohesion properties of Fe/W interfaces.

In addition, the interface energy (E_{int}), which is the energy of obtaining the interface from bulk materials, is also computed by the following form:

$$E_{int} = \frac{E_{tot} - E_{bulk-Fe} - E_{bulk-W}}{2A} \quad (8)$$

Here, E_{tot}, $E_{bulk-Fe}$ and E_{bulk-W} are bulk energies of the interface, overlayer, and substrate, respectively.

Table 2 – Work of separation W_{sep} (J/m^2) and interface energy E_{int} (J/m^2) of interstitial hydrogen at (100)Fe/(100)W interface. The changes of work of separation (ΔW_{sep}) and interface energy (ΔE_{int}) as a reference of pure Fe/W interface ($W_{sep} = 6.283$ J/m^2 and $E_{int} = 0.131$ J/m^2) are also listed for the sake of comparison.

H location	W_{sep} (J/m^2)	ΔW_{sep} (J/m^2)	E_{int} (J/m^2)	ΔE_{int} (J/m^2)
T1	6.166	−0.117	0.248	0.117
T2	5.934	−0.349	0.48	0.349
T5	6.314	0.031	0.1	−0.031
O1	6.469	0.186	−0.055	−0.186
O2	5.887	−0.396	0.527	0.396
O4	6.117	−0.166	0.297	0.166
O6	6.445	0.162	−0.031	−0.162

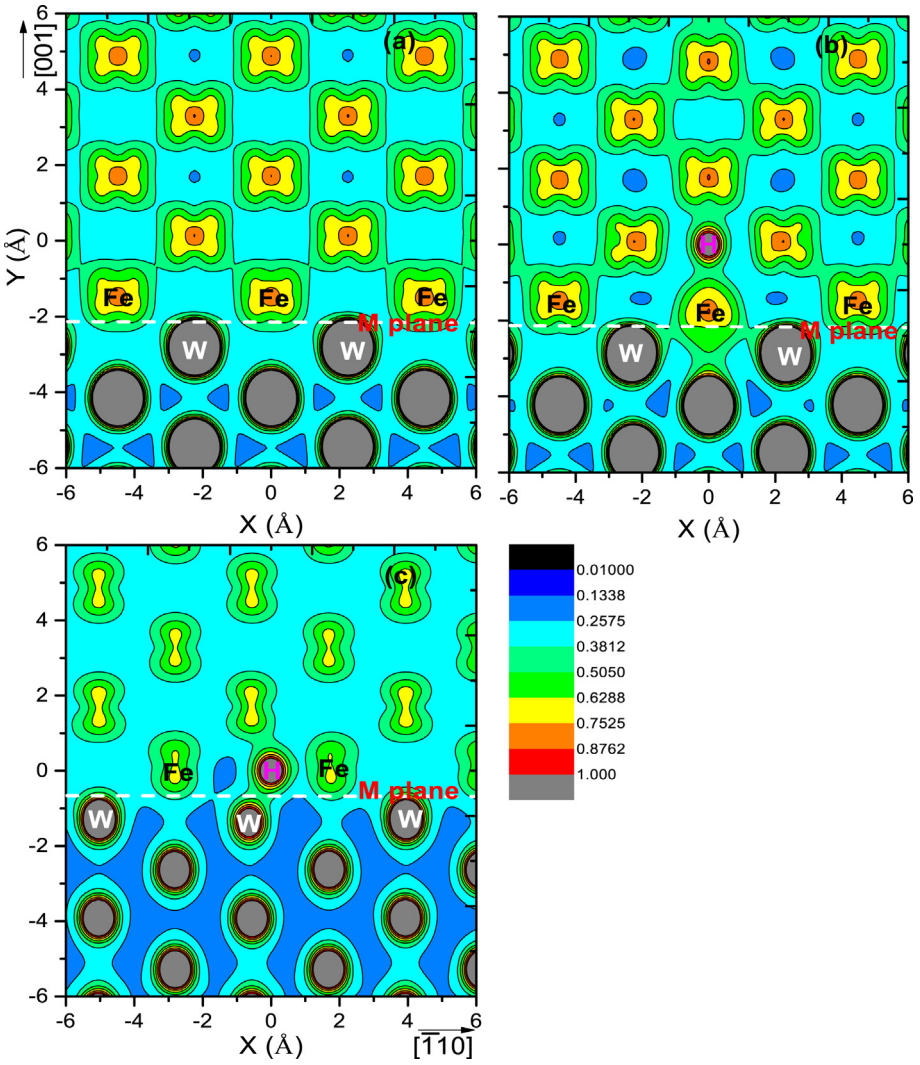

Fig. 5 – Charge density plots of (a) pure (100)Fe/(100)W interface, and hydrogen at (b) O1 and (c) T2 sites, respectively.

The E_{int} values of H at all the seven sites of (100)Fe/(100)W interface are derived and listed in Table 2, too. As a reference, we also calculated the changes of interface energy (ΔE_{int}) of pure interface ($E_{int} = 0.131\ J/m^2$). Such a small E_{int} value of pure (100)Fe/(100)W interface also matches well with the similar experimental observations and computational data in the literatures [12,38,39]. It could be discerned clearly from this table that H at the sites of T1, T2, O2 and O4 with positive ΔE_{int} values would decrease interface stability. It's worth mentioning that the sites of T2 and O2 are about 0.35 J/m^2 higher than the pure interface, predicting that dissolving H at W layer of the interface seems to bring about the significant decrease of interface stability. Last, one conclusion from Table 2 is that the E_{int} has a strong correlation with the W_{sep}, i.e., a lower E_{int} means a higher interfacial strength, and vice versa.

It is essential to understand the effects of H on interface cohesion, and Fig. 5, as the second example, demonstrates the comparison of electron distribution maps of pure (100)Fe/(100)W interface and the interface with H at T2 and O1 sites in (110) plane. As shown in Fig. 5(a) and (b), bigger charge densities and stronger bonds of W–Fe have been found in (b), implying that the dissolving H at the O1 site can increase metallic bonding of several W–Fe bonds between Fe and W layers. Thus, the interface with H at O1 site has more charge accumulation and stronger interaction. Moreover, it also can be seen from Fig. 5(a) and (c) that the charge densities within the pure interface seem a little bit denser than those of H at the T1 site, which could therefore bring about a deep understanding to the weaker interface cohesion of H at T1 site.

Conclusions

In summary, first-principles study has been used to systematically reveal the mechanism of bubble formation and cohesion properties of hydrogen at (100)Fe/(100)W interfaces. Our calculations reveal that the T5 site of the interface has a negative binding energy. Such a phenomenon predicts the generated hydrogen would rapidly accumulate at T5 site during the process of fusion reactions. Then, according to first-principles study with Sievert's law, we calculated and obtained temperature-dependent solubility of hydrogen at Fe/W interfaces, as well as W and Fe bulks. A probably useful insight into the descending sequence of hydrogen bubble

formation is as follows: Fe/W interface → Fe bulk → W bulk. Moreover, the effects of hydrogen on interface cohesion are discussed and clarified. It is found that H at the sites of O1 and O6 relatively far away from M plane could significantly increase interface strength, while H at the sites of T2 and O2 of W layer would bring about the significant decrease of interface stability. The calculated results not only agree well with similar experimental observations in the literature, but also make reasonable interpretations of hydrogen at Fe/W interfaces by electronic distributions, which could be used as a guiding parameter for design of plasma-facing components.

Acknowledgment

This research work was supported by National Natural Science Foundation of China (Grant No. 21571095, 61366004 and 51362020).

REFERENCES

[1] Linsmeier C, Rieth M, Aktaa J, Chikada T, Hoffmann A, Hoffmann J, et al. Development of advanced high heat flux and plasma-facing materials. Nucl Fusion 2017;57. 092007.
[2] Pitts RA, Carpentier S, Escourbiac F, Hirai T, Komarov V, Lisgo S, et al. A full tungsten divertor for ITER: physics issues and design status. J Nucl Mater 2013;438. S48-56.
[3] Ueda Y, Schmid K, Balden M, Coenen JW, Loewenhoff TW, Ito A, et al. Baseline high heat flux and plasma facing materials for fusion. Nucl Fusion 2017;57. 092006.
[4] Wurster S, Baluc N, Battabyal M, Crosby T, Du J, García-Rosales C, et al. Recent progress in R&D on tungsten alloys for divertor structural and plasma facing materials. J Nucl Mater 2013;442:S181–9.
[5] Yih SWH, Wang CT. Tungsten-sources, metallurgy, properties and applications. New York: Plenum Press; 1979.
[6] Solntceva E, Taubin M, Bochkov N, Solntsev V, Yaskolko A. Use of tungsten single crystals to enhance nuclear reactors structural elements properties. Int J Hydrogen Energy 2016;41:7206–12.
[7] Chen L, Fan JL, Gong HR. Phase transition and mechanical properties of tungsten nanomaterials from molecular dynamics simulation. J Nanoparticle Res 2017;19:118.
[8] Gilbert MR, Sublet JC. Neutron-induced transmutation effects in W and W-alloys in a fusion environment. Nucl Fusion 2011;51. 043005.
[9] Thomas G, Vincent R, Matthews G, Dance B, Grant P. Interface topography and residual stress distributions in W coatings for fusion armour applications. Mater Sci Eng A 2008;477:35–43.
[10] Basuki WW, Aktaa J. Investigation on the diffusion bonding of tungsten and EUROFER97. J Nucl Mater 2011;417:524–7.
[11] Nahm TU, Gomer R. The conversion of Fe on W(110) from the low temperature to the high temperature form. Surf Sci 1997;373:237–56.
[12] Ren QQ, Fan JL, Gong HR. Work function and cohesion properties of W-Fe interfaces. Mater Lett 2015;145:205–8.
[13] Bagchi S, Jani S, Anwar S, Lakshmi N, Lalla N. Structural and magnetic study of swift heavy ion irradiated W/Fe multilayer structure. J Magn Magn Mater 2010;322:3851–6.
[14] Joseph-Auguste C, Cheikhravat H, Djebaili-Chaumeix N, Deri E. On the use of spray systems: an example of R&D work in hydrogen safety for nuclear applications. Int J Hydrogen Energy 2009;34:5970–5.
[15] Jia YZ, Liu W, Xu B, Qu SL, Shi LQ, Morgan TW, et al. Subsurface deuterium bubble formation in W due to low-energy high flux deuterium plasma exposure. Nucl Fusion 2017;57. 034003.
[16] Marian J, Becquart CS, Domain C, Dudarev SL, Gilbert MR, Kurtz RJ, et al. Recent advances in modeling and simulation of the exposure and response of tungsten to fusion energy conditions. Nucl Fusion 2017;57. 092008.
[17] Ikeda K, Otsuka T, Tanabe T. Determination of hydrogen diffusivity and permeability in W near room temperature applying a tritium tracer technique. J Nucl Mater 2011;415:S684–7.
[18] Benamati G, Serra E, Wu CH. Hydrogen and deuterium transport and inventory parameters through W and W-alloys for fusion reactor applications. J Nucl Mater 2000;283–287:1033–7.
[19] Shu WM, Wakai E, Yamanishi T. Blister bursting and deuterium bursting release from tungsten exposed to high fluences of high flux and low energy deuterium plasma. Nucl Fusion 2007;47:201–9.
[20] Liu YL, Zhang Y, Zhou HB, Lu GH. Vacancy trapping mechanism for hydrogen bubble formation in metal. Phys Rev B 2009;79. 172103.
[21] Kresse G, Hafner J. Ab initio molecular dynamics for liquid metals. Phys Rev B 1993;47:558–61.
[22] Chen L, Wang Q, Xiong L, Gong HR. Mechanical properties and point defects of MC (M=Ti, Zr) from first-principles calculation. J Alloy Comp 2018;747:972–7.
[23] Perdew JP, Chevary JA, Vosko SH, Jackson KA, Pederson MR, Singh DJ, et al. Atoms, molecules, solids, and surfaces: applications of the generalized gradient approximation for exchange and correlation. Phys Rev B 1992;46:6671–87.
[24] Perdew JP, Burke K, Ernzerhof M. Perdew, burke, and ernzerhof reply. Phys Rev Lett 1998;80:891.
[25] Kresse G, Joubert J. From ultrasoft pseudopotentials to the projector augmented-wave method. Phys Rev B 1999;59:1758–75.
[26] Methfessel M, Paxton AT. High-precision sampling for Brillouin-zone integration in metals. Phys Rev B 1989;40:3616–21.
[27] Wang Q, Chen L, Xiong L, Gong HR. Mechanical and thermodynamic properties of cubic boron nitride from ab initio calculation. J Phys Chem Solids 2017;104:276–80.
[28] Chen L, Fan JL, Song M, Gong HR. Structural stability and magnetic properties of WFeH phases. Int J Hydrogen Energy 2016;41:13093–100.
[29] Besenbacher F, Myers SM, Nordlander P, Norskov JK. Multiple hydrogen occupancy of vacancies in Fe. J Appl Phys 1987;61:1788–94.
[30] Han QF, Liu YL, Zhang Y, Ding F, Lu GH. A theoretical insight into H accumulation and bubble formation by applying isotropic strain on the W-H system under a fusion environment. Nucl Fusion 2018;58. 046014.
[31] Jiang B, Wan FR, Geng WT. Strong hydrogen trapping at helium in tungsten: density functional theory calculations. Phys Rev B 2010;81. 134 112.
[32] Kong XS, Wang S, Wu XB, You YW, Liu CS, Fang QF, et al. First-principles calculations of hydrogen solution and diffusion in tungsten: temperature and defect-trapping effects. Acta Mater 2015;84:426–35.
[33] Frauenfelder R. Solution and diffusion of hydrogen in tungsten. J Vac Sci Technol 1969;6:388–97.
[34] Liu LC, Wang JW, Qian J, He YH, Gong HR, Liang CP, et al. Fundamental effects of Ag alloying on hydrogen behaviors in PdCu. J Membe Sci 2018;550:230–7.

[35] Chen L, Wang Q, Jiang WG, Gong HR. Hydrogen solubility in Pd_3Ag phases from first-principles calculation. Metals 2019;9:121.
[36] Tang W, Sanville E, Henkelman G. A grid-based Bader analysis algorithm without lattice bias. J Phys Condens Matter 2009;21. 084204.
[37] Chen X, Chen XR, Hou TZ, Li BQ, Cheng XB, Zhang R, et al. Lithiophilicity chemistry of heteroatom-doped carbon to guide uniform lithium nucleation in lithium metal anodes. Sci Adv 2019;5. eaau7728.
[38] Yang JX, Chen L, Fan JL, Gong HR. Doping of helium at Fe/W interfaces from first principles calculation. J Alloy Comp 2016;686:160–7.
[39] Schmidt R, Schwarz A, Wiesendanger R. Magnetization switching utilizing the magnetic exchange interaction. Phys Rev B 2012;86. 174402.